lung collapse and gas insufflation). To determine the effects of lung collapse and insufflation, this port site selection algorithm could be applied to registered sequential images while using varying levels of chest insufflation. Both of these examples (anatomic extremes and chest insufflation) represent important elements of future validation work.

Thus, pending further validation, this algorithmic approach may improve the efficiency and safety of robot-assisted CABG by optimizing placement of the instrument and endoscope ports. Implementation of this algorithm for robot-assisted CABG and similar algorithms for other robot-assisted procedures could assist surgeons in transitioning to telesurgical techniques while ensuring the best possible clinical outcome from these procedures.

ACKNOWLEDGMENT

The authors gratefully acknowledge the technical assistance of J. Titus and Dr. J. White in the MGH Cardiovascular Surgery Laboratory.

REFERENCES

[1] H. A. Tabaie, J. A. Reinbolt, W. P. Graper, T. F. Kelly, and M. A. Connor, "Endoscopic coronary artery bypass graft (ECABG) procedure with robotic assistance," *Heart Surgery Forum*, vol. 2, pp. 310–315, 1999.

[2] W. D. Boyd *et al.*, "Closed-chest coronary artery bypass grafting on the beating heart with the use of a computer-enhanced surgical robotic system," *J. Thoracic Cardiovascular Surgery*, vol. 120, pp. 807–809, 2000.

[3] U. Kappert *et al.*, "Development of robotic enhanced endoscopic surgery for the treatment of coronary artery disease," *Circulation*, vol. 104, no. Suppl. 1, pp. 102–107, 2001.

[4] M. Argenziano, "Columbia-Presbyterian minimally invasive and robotic cardiac surgery program," in *Engineering the Future of Surgery: Symp. for Surgeons and Engineers*, New York, NY, 2002.

[5] D. Loulmet *et al.*, "Endoscopic coronary artery bypass grafting with the aid of robotic assisted instruments," *J. Thoracic Cardiovascular Surgery*, vol. 118, pp. 4–10, 1999.

[6] G. Lehmann *et al.*, "Toward dynamic planning and guidance of minimally invasive robotic cardiac bypass surgical procedures," in *Proc. MICCAI 2001*, Utrecht, The Netherlands, 2001, pp. 368–375.

[7] A. Chiu, D. Day, M. Drangova, D. Boyd, and T. Peters, "3-D image guidance for minimally invasive robotic coronary artery bypass," *Heart Surgery Forum*, vol. 3, pp. 224–231, 2000.

[8] L. Adhami, E. Coste-Manière, and J.-D. Boissonnat, "Planning and simulation of robotically assisted minimal invasive surgery," in *Proc. Medical Image Computing and Computer Assisted Intervention-MICCAI 2000*, Pittsburgh, PA, 2000, pp. 624–633.

[9] E. Coste-Manière *et al.*, "Optimized port placement for the totally endoscopic coronary artery bypass grafting using the Da Vinci robotic system," in *Lecture Notes in Control and Information Sciences, Experimental Robotics VII*, D. Russ and S. Singh, Eds. Berlin: Springer-Verlag, 2001, vol. 271, pp. 199–208.

[10] R. J. Damiano *et al.*, "Initial prospective multicenter clinical trial of robotically-assisted coronary artery bypass grafting," *Ann. Thoracic Surgery*, vol. 72, pp. 1263–1269, 2001.

[11] P. Oppenheimer *et al.*, "Laparoscopic surgical simulator and port placement study," *Studies Health Technol. Inform.*, vol. 70, pp. 233–235, 2000.

[12] G. B. Hanna, S. Shimi, and A. Cuschieri, "Optimal port locations for endoscopic intracorporeal knotting," *Surgical Endoscopy*, vol. 11, pp. 397–401, 1997.

[13] ——, "Influence of direction of view, target-to-endoscope distance and manipulation angle on endoscopic knot tying," *British J. Surgery*, vol. 84, pp. 1460–1464, 1997.

[14] S. Selha, "Dexterity optimization through port placement in robot-assisted minimally invasive surgery," Master's thesis, Dept. Aero. Mech. Eng., Boston Univ., Boston, MA, 2002.

[15] C. Wagner, N. Stylopoulos, and R. Howe, "The role of force feedback in surgery: Analysis of blunt dissection," in *Proc. 10th Int. Symp. Haptic Interfaces for Virtual Environment and Teleoperator Systems*, Orlando, FL, 2002, pp. 73–79.

[16] J. Cannon, R. Howe, P. Dupont, J. Triedman, G. Marx, and P. del Nido, "Application of robotics in congenital cardiac surgery," in *Proc. Seminar Thoracic Cardiovascular Surgery: Pediatric Cardiac Surgery Ann.*, vol. 6, 2003, pp. 72–83.

A Miniature Microsurgical Instrument Tip Force Sensor for Enhanced Force Feedback During Robot-Assisted Manipulation

Peter J. Berkelman, Louis L. Whitcomb, Russell H. Taylor, and Patrick Jensen

***Abstract*—This paper reports the development of a new miniature force sensor designed to measure contact forces at the tip of a microsurgical instrument in three dimensions, and its application to scaled force feedback using a cooperatively manipulated microsurgical assistant robot. The principal features of the sensor are its small size of 12.5 mm in diameter and 15 mm in height, a novel configuration of flexure beams and strain gauges in order to measure forces isotropically at the instrument tip 40 mm from the sensor body, and sub-mN three-axis force-sensing resolution.**

***Index Terms*—Clinical human computer interfaces, force sensor, microelectromechanical systems (MEMS)-based medical devices, robotics and robotic manipulators.**

I. INTRODUCTION

This paper reports the design, implementation, and testing of a miniature force sensor developed to measure forces in three dimensions at the tip of a microsurgical instrument. The miniature force sensor is designed to be mounted inside a handheld instrument or compact robot end-effector in order to measure the forces at the tip of the instrument in all three axes with sub-mN resolution. The use of two sets of crossed beams as the elastic elements in the force sensor provides uniform stiffness as measured with respect to the tool tip coordinate frame, located 40 mm from the body of the force sensor. We report the application of this force sensor, in combination with a second sensor, to perform robotically assisted 62.5:1 amplified force reflection for micromanipulation.

Microsurgical force measurement experiments reported in [1] show that typical forces on microsurgical instrument tips during retinal surgery are less than 7.5 mN, below the threshold of the operator's tactile sensitivity. Measurement and comparison of hand tremor, both while holding microsurgical instruments in a fixed position and during

Manuscript received January 16, 2003; revised April 25, 2003 and July 16, 2003. This paper was recommended for publication by Associate Editor P. Dupont and Editor A. De Luca upon evaluation of the reviewers' comments. This work was supported in part by the National Science Foundation under Grant IIS9801684 and Grant EEC9731478, in part by the National Institutes of Health under Training Grant 5-T32-HL07712, and in part by internal funding from The Johns Hopkins University.

P. J. Berkelman is with the TIMC-IMAG Laboratory, Institut Albert Bonniot, 38706 La Tronche, France (e-mail: peter.berkelman@imag.fr).

L. L. Whitcomb is with the Mechanical Engineering Department, The Johns Hopkins University, Baltimore, MD 21218 USA.

R. H. Taylor is with the Engineering Research Center for Computer Integrated Surgical Systems and Technology, The Johns Hopkins University, Baltimore, MD 21218 USA.

P. Jensen is with Advanced Imaging Technologies, Inc., Preston, WA 98050 USA.

Digital Object Identifier 10.1109/TRA.2003.817526

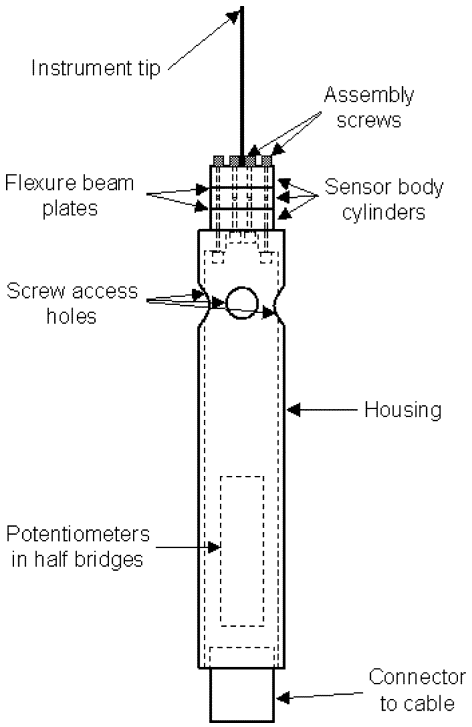

Fig. 1. Sensor with instrument tip and housing.

task performance, was reported in [2] and [3]. These studies indicate a lower bound in human tool positioning accuracy of 20–40 μm during microsurgery. Based on these results, we believe that retinal microsurgeons operate using visual feedback with little or no tactile sensing feedback through the instruments. If a robotic force amplification system could amplify these small contact forces to enable a surgeon to directly sense microsurgical forces, it may significantly increase safety, minimize damage to tissues, improve outcomes of existing procedures, and may enable new procedures not presently feasible.

II. Tip Force Sensor Design

The design goals of the new sensor were determined through evaluation of microsurgical manipulation performance and size requirements, finite element analysis of strain levels in response to sensor loads, and considerations of cost and ease of assembly. The sensor must fit on the handle of a typical microsurgical instrument and measure forces at the instrument tip in all directions with sub-mN resolution. Our design goals were as follows.

Force Range: ± 1.0 N.
Force Resolution: 0.5 mN.
Overload Limit: 5.0 N.
Sensor Diameter: 12.5 mm.
Sensor Height: 15 mm.
Instrument Tip Length: 40 mm.

The overall shape of the sensor consists of an outer hollow cylinder joined to an inner cylinder by eight thin flexible beams. Each flexure beam is 0.5 mm wide, 0.125 mm thick, and 3.0 mm long. The beams extend radially from the inner cylinder to the inside wall of the outer cylinder and are arranged in two separate layers in a double-cross configuration. The outer cylinder is attached to the body of the instrument and the extended tip is mounted in the inner cylinder, as seen in Fig. 1. Silicon strain gauges[1] are bonded to the outer end of each beam and connected in half bridges.

[1]Micron Instruments SS-060-033-500PU

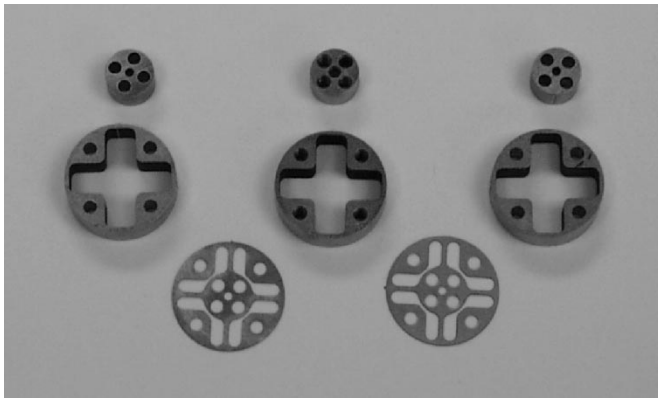

Fig. 2. Force sensor components.

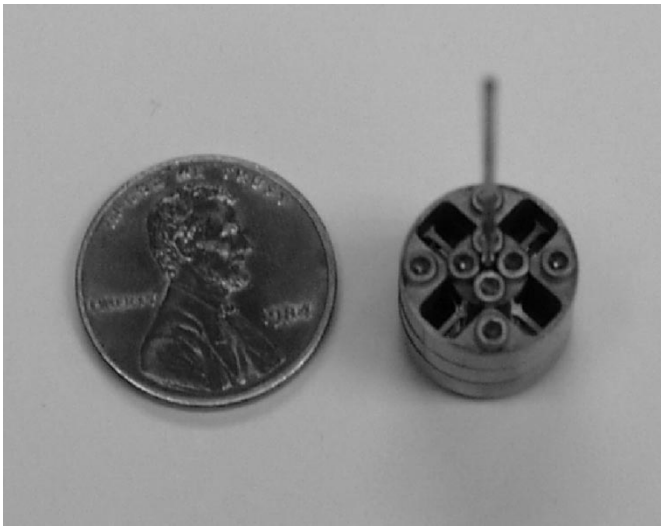

Fig. 3. Assembled sensor.

The metal parts of the sensor are joined together in layers, as shown in Figs. 2 and 3. The sensor parts are 400 series stainless steel and the fasteners are ASTM standard A574/F835 alloy steel. The parts of the miniature force sensor were fabricated using wire-cut electrical discharge machining (EDM) to achieve consistent tolerances at sub-mm dimensions without residual stresses, warping, or burrs that may be caused by conventional machining.

A. Double-Cross Flexure Beam Configuration

Typical conventional multiaxis force sensors contain a set of elastic beams arranged in a cross configuration and instrumented with strain gauges. To obtain a tool tip sensor with isotropic sensitivity, we have developed a double cross design with two vertically separated flexure beam crosses, as originally suggested but not implemented in [4]. The double-cross flexure beam configuration adds stiffness in response to torques from radial forces at the tip but not to axial forces, so the sensor can be made uniformly sensitive to forces in all directions at the instrument tip by varying the vertical separation between the beam crosses. In this design, the sensor sensitivity to axial and nonaxial forces was equalized by a 4.0-mm separation.

B. Strain Measurement

The average strain in a region on a flexed beam on the force sensor is measured by bonding a strain gauge to the surface of the beam and measuring the change in its resistance as the sensor is loaded. Multiple

gauges are typically wired together in a half or full bridge configuration to reduce the effects of changes in temperature and magnify the measurable signal.

The maximum beam strains in the finite element model of the sensor with a 1.0 N radial force at the instrument tip are approximately $\pm 500\ \mu\epsilon$, well within the operating range of the gauges. The safety factors for the normal and shear stress yield points of the sensor beams are in the 3–4 range to avoid any plastic deformation of the beams.

The sensor contains eight strain gauges in four half bridges. Each gauge is paired with its counterpart on the other flexure beam cross. The instrument tip forces vary with the strain gauge half-bridge voltages approximately as follows:

$$f_x \approx \frac{C(\Delta V_1 - \Delta V_3)}{2} \tag{1}$$

$$f_y \approx \frac{C(\Delta V_2 - \Delta V_4)}{2} \tag{2}$$

$$f_z \approx \frac{C(\Delta V_1 + \Delta V_2 + \Delta V_3 + \Delta V_4)}{4} \tag{3}$$

where each ΔV refers to the change in voltage from the unloaded condition for each strain gauge pair, and C is an empirically determined scaling factor. To obtain accurate force measurements, the sensor must be calibrated to correct for variations in strain gauge mounting locations, gauge resistances, and beam dimensions.

The strain gauge bridge amplifier gains were set to 250 V/V to obtain a ± 10.0 V range output signal from sensor loads up to 50 g. The excitation voltage was set to 5.0 V to obtain stable output signals without overheating the strain gauges. The amplifiers internally balance the strain gauge bridges so that offsets in the strain gauge signals due to thermal variations and the weight of the instrument tip in a given orientation can be eliminated by rezeroing the amplifier output. Due to the limited balance range of the internal half bridges in the signal conditioning amplifiers, a 100-Ω potentiometer, mounted inside the housing as shown in Fig. 1, is included in each half bridge circuit of the sensor for coarse bridge, balancing to within $\pm 1\ \Omega$.

C. Calibration

A calibration procedure is necessary to calculate a linear matrix transform between the strain gauge bridge signals and the three–dimensional (3-D) force load vector. To obtain sensor calibration data, 10, 20, 30, 40, and 50 g weights were suspended from the tip of the instrument in different orientations to apply loads in the $+x$, $-x$, $+y$, $-y$, and $-z$ directions. Given the matrix of sensor bridge signals $\boldsymbol{S}$ in volts and the corresponding matrix of sensor loads $\boldsymbol{F}$ in newtons, the linear transformation $\boldsymbol{A}$ between them in

$$\boldsymbol{F} = \boldsymbol{A}\boldsymbol{S} \tag{4}$$

can be determined by calculating the Moore–Penrose least-squares error solution to the overdetermined set of equations. This calibration procedure produced the sensor signals in Fig. 4, shown in volts as a function of sensor load in newtons. The least-squares transformation calculated from the calibration data is

$$\boldsymbol{A} = \begin{bmatrix} -0.0054 & -0.0277 & -0.0069 & 0.0392 \\ 0.1028 & -0.0769 & 0.0326 & -0.0841 \\ -0.0568 & 0.0870 & -0.0516 & 0.1024 \end{bmatrix}.$$

This mapping differs from the expected mapping for the sensor described in Section II-B due to residual stresses from assembly and material and dimensional variations in the sensor components. The maximum error of the fabricated sensor due to nonlinearity in the calibrated ± 0.5 N range when the least-squares transformation $\boldsymbol{A}$ applied is 0.013 N or 2.7%.

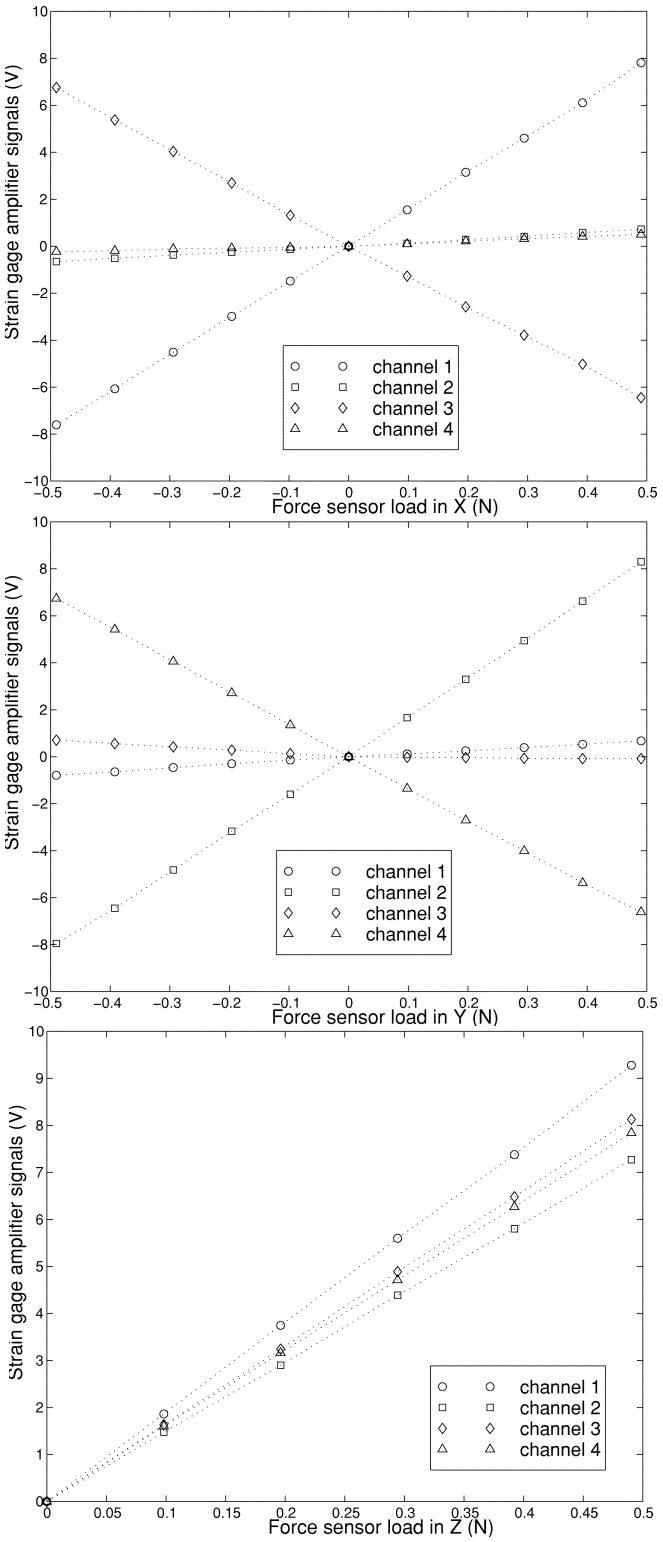

Fig. 4. Force sensor calibration data in X, Y, and Z directions with amplified strain gauge bridge output in volts as a function of applied calibration force in newtons.

D. Output Characterization

The y ouput of the force sensor, fed through a 10-Hz lowpass antialiasing filter and sampled at 100 Hz while under load is shown in Fig. 5. The standard deviation or root mean square (rms) error of this filtered signal is 0.49 mN. As is typical of silicon strain gauges, $1/f$

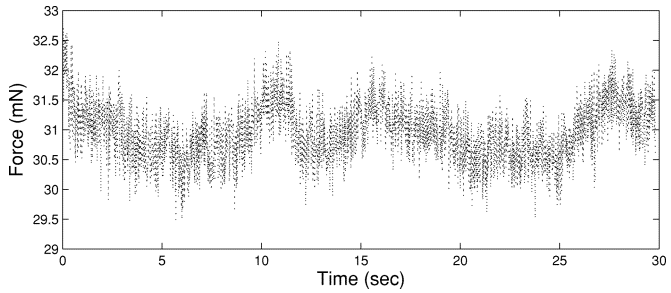

Fig. 5. Typical sensor signal noise and drift in millinewtons against time in seconds.

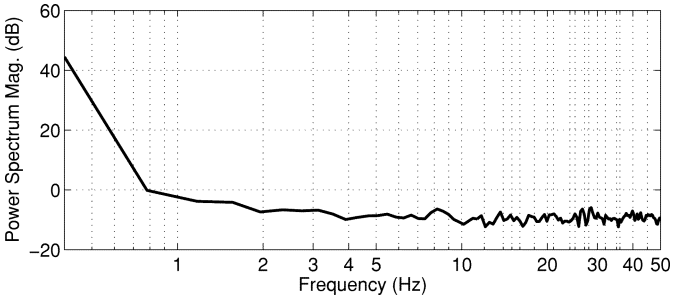

Fig. 6. Power spectral density of signal noise of Fig. 5.

noise is present in the sensor output at low frequencies. The power spectral densities of the y output of the sensor are shown in Fig. 6.

Variations in strain gauge resistance can arise from thermal expansion of the flexure beams, the thermal coefficients of resistance and gauge factor of the silicon gauges, and the gauge/beam interaction via the intervening layer of insulator and epoxy binding material. We employed a balanced half-bridge gauge configuration to minimize the effect of uniform changes in the temperature of the sensor as a whole. Temperature variations *between* strain gauges may have a significant effect on the sensor output, however. The gauges generate heat from resistive heating, and the two gauges of each half bridge are separated by 4 mm and may be subject to differences in convective and conductive heat transfer. Heating from the user's hand is expected to be minimal as there is an insulating air gap between the outer surface of the handle and the housing of the tip force sensor.

The calibration and experimental trials of this prototype sensor reported in this short paper were performed at thermal equilibrium at room temperature with no temperature compensation. For general microsurgical use, the effects of thermal variation on the strain gauge output should be precisely characterized via calibration experiments in a thermal chamber. The resulting data would enable compensation of the sensor output for the effects of thermal variation.

III. Experimental Force Scaling Application

Our steady-hand surgical assistant robot has a modular design with a three degree-of-freedom (DOF) linear translation stage, a 2-DOF remote center of rotation module [5], and a tool insertion and rotation stage [6]. It provides position-controlled motion with micrometer resolution. The maximum position control bandwidth of the joint actuators is 20–25 Hz. Force control is implemented at a sample rate of 100 Hz as an added layer above the position controller by updating the desired velocity in the joint controllers as follows:

$$f_{\rm des} = \frac{f_{\rm handle}}{C} + f_{\rm offset} \tag{5}$$

$$\dot{x}_{\rm des} = K(f_{\rm des} - f_{\rm tip}) \tag{6}$$

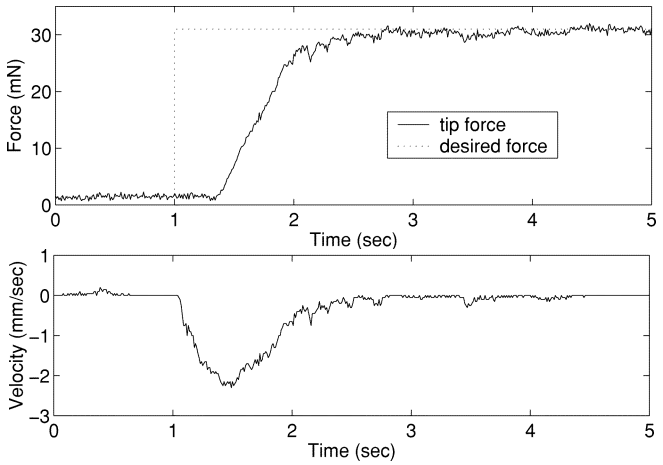

Fig. 7. Force control step response using sensor force in Newtons and robot motion velocity in millimeters/second as a function of time in seconds.

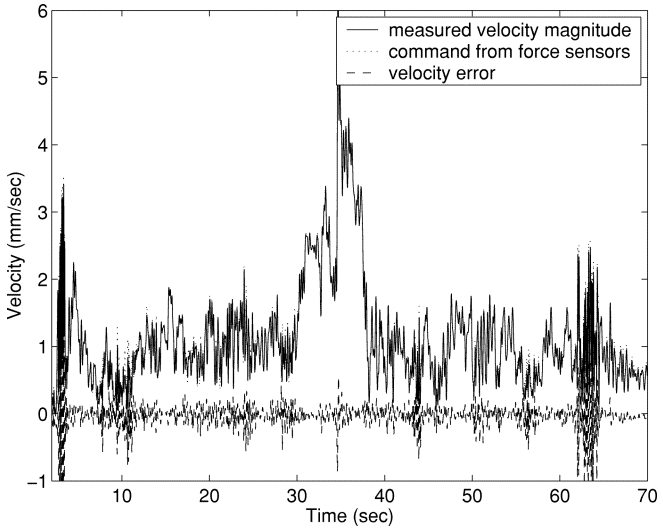

Fig. 8. Desired and measured instrument tip velocity absolute value as a function of time in seconds during scaled force feedback control as tip is moved against a suspended sheet of paper.

so that tip contact forces are scaled up for the user and the response of the robot is purely viscous when there is no tip contact force, as typical for "hands on" or "cooperatively manipulated" robot assistants [7]–[11]. In this controller, $\dot{x}_{\rm des}$ is the desired end-effector velocity, K is the force-to-velocity control gain, C is the force scaling factor, $f_{\rm tip}$ is the sensed force at the instrument tip, $f_{\rm handle}$ is the user manipulation force sensed on the instrument handle, and $f_{\rm offset}$ is the desired resting tip force, set to zero during typical manipulation tasks. Adaptive force control methods as presented by Roy and Whitcomb [12] may also be implemented on this manipulator. This robotic system is based on the "steady hand" cooperative manipulation paradigm, in which the surgeon and the robot both hold a microsurgical instrument and the robot end-effector to the sensed manipulation forces of the surgeon's hand on the instrument [7], [8].

For scaled force reflection, both user manipulation and instrument tip interaction forces must be sensed independently. In this study, a ring-shaped commercial six-axis force sensor[2] is used to measure the user's forces and torques on a handle while the miniature sensor measures forces at the instrument tip. Preliminary results with "steady hand" interactive force scaling were reported in [13] and [14] with motion and sensing along a single axis. To test steady-hand force

[2]ATI Industrial Automation Nano43

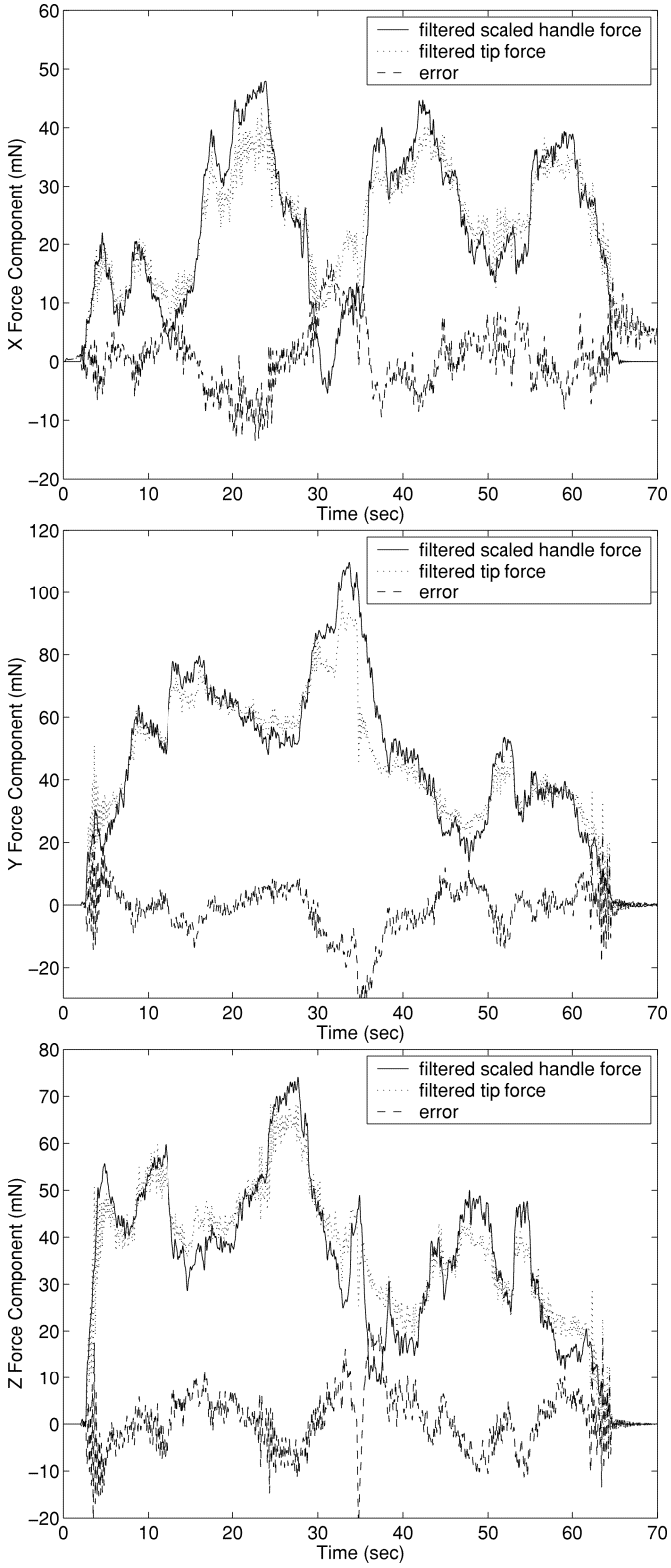

Fig. 9. X, Y, and Z force components in newtons as a function of time in seconds during scaled force feedback control.

scaling control in all directions with the new sensor, a sheet of paper was suspended horizontally within the workspace of the robot to simulate bodily tissue. The handle-to-tip force scaling factor C was 62.5:1 for both hand-manipulated trajectories and force-command step responses, and the force-to-velocity viscous response gain K was 0.12 m/s/N.

Fig. 7 shows the force control response to a step input, given by hanging a 200 g weight from the instrument handle on the steady-hand robot. The delay in the force response occurs as the instrument tip is moved by the robot to the point where the force from the deflection of the paper sheet equals the commanded force.

In this steady-hand scaled force feedback experiment shown in Figs. 8 and 9, the paper was palpated with the tip of the instrument held by both user and robot. In Fig. 8, the commanded and measured velocities mostly overlay each other. The rotation DOF of the robot were also active during the experiment. Aside from high-frequency variation due to vibration of the robot, the measured tip force is equivalent to the scaled handle force trajectory and an added term proportional to the velocity of the tip, as expressed in the control law of (6). Equivalently, the user forces on the handle contribute to both the robot end-effector velocity and the tip force, so that the commanded tip velocity is proportional to the difference between the desired and measured tip forces. The larger force feedback errors shown between 30-40 s are due to the high velocity of the force sensor tip, as shown in Fig. 8. The remaining errors, generally less than 10 mN, are primarily due to the low bandwidth of the robot controller, which limits the response to higher frequencies in the command force. Nevertheless, at the slower frequencies of interest in microsurgery, the robot reacts to changes in the tip force of less than 5 mN, amplifying these forces with a gain of 62.5 to the instrument handle, enabling the user to perceive these changes easily, whereas they would be imperceptible without amplified force feedback.

ACKNOWLEDGMENT

The authors gratefully acknowledge the contributions and assistance of the following: D. Stoianovici and the Johns Hopkins URobotics Laboratory for the remote center-of-motion module of the robot, J. Burns and the Johns Hopkins Biomedical Engineering Instrument Shop for parts fabrication, T. Shelley for fabrication advice, and Dr. E. de Juan, M.D. and the MADLab for additional advice and support.

REFERENCES

[1] P. K. Gupta, P. S. Jensen, and E. deJuan, Jr., "Surgical forces and tactile perception during retinal microsurgery," in *Medical Image Computing and Computer-Assisted Interventions (MICCAI)*. Cambridge, U.K.: Springer, 1999, vol. 1679, Lecture Notes in Computer Science, pp. 1218–1225.

[2] M. Gomez-Blanco, C. Riviere, and P. Khosla, "Intraoperative instrument motion sensing for microsurgery," in *Proc. 21st Conf. IEEE Engineering in Medicine and Biology Society*, Oct. 1999, p. 864.

[3] C. N. Riviere, R. S. Rader, and P. K. Khosla, "Characteristics of hand motion of eye surgeons," in *Proc. 19th Conf. IEEE Engineering in Medicine and Biology Society*, Chicago, IL, Oct. 1997, pp. 1690–1693.

[4] D. Reynaerts, J. Piers, and H. van Brussel, "A mechatronic approach to microsystem design," *IEEE/ASME Trans. Mechatron.*, vol. 3, pp. 24–33, Mar. 1998.

[5] D. Stoianovici, L. L. Whitcomb, J. Anderson, R. H. Taylor, and L. R. Kavoussi, "A modular surgical robotic system for image-guided percutaneous procedures," in *Medical Image Computing and Computer-Assisted Intervention (MICCAI)*. Cambridge, MA: Springer, 1998, vol. 1496, Lecture Notes in Computer Science, pp. 404–410.

[6] R. H. Taylor, P. Jensen, L. Whitcomb, A. Barnes, R. Kumar, D. Stoianovici, P. Gupta, Z. Wang, E. deJuan, and L. Kavoussi, "A steady-hand robotic system for microsurgical augmentation," in *Medical Image Computing and Computer-Assisted Interventions (MICCAI)*. Cambridge, U.K.: Springer, 1999, vol. 1679, Lecture Notes in Computer Science, pp. 1031–1041.

[7] R. H. Taylor, J. Funda, B. Eldridge, K. Gruben, D. LaRose, S. Gomory, and M. Talamini, "A telerobotic assistant for laparoscopic surgery," in *Computer-Integrated Surgery*, R. H. Taylor, S. Lavallée, G. C. Burdea, and R. Mosges, Eds. Cambridge, MA: MIT Press, 1996, ch. 45, pp. 581–592.

[8] R. H. Taylor, H. A. Paul, P. Kazandzides, B. D. Mittelstadt, W. Hanson, J. F. Zuhars, B. Williamson, B. L. Musits, E. Glassman, and W. L. Bargar, "An image-directed robotics system for precise orthopedic surgery," *IEEE Trans. Robot. Automat.*, vol. 10, pp. 261–275, June 1994.

[9] S. J. Harris, W. J. Lin, K. L. Fan, R. D. Hibberd, J. Cobb, R. Middleton, and B. L. Davies, "Experiences with robotic systems for knee surgery," in *Proc. 1st Joint Conf. CVRMed and MRCAS*, Grenoble, France, 1997, pp. 756–766.

[10] S. C. Ho, R. D. Hibberd, and B. L. Davies, "Robot assisted knee surgery," *IEEE Eng. Med. Bio. Mag. Special Issue Robot. Surgery*, pp. 292–300, Apr. 1995.

[11] J. Troccaz, M. Peshkin, and B. L. Davies, "The use of localizers, robots and synergistic devices in CAS," in *Proc. 1st Joint Conf. CVRMed and MRCAS*, Grenoble, France, 1997, pp. 727–729.

[12] J. Roy and L. L. Whitcomb, "Adaptive force control of position/velocity controlled robots: Theory and experiment," *IEEE Trans. Robot. Automat.*, vol. 18, pp. 121–137, Apr. 2002.

[13] R. Kumar, P. Berkelman, P. Gupta, A. Barnes, P. Jensen, L. Whitcomb, and R. Taylor, "Preliminary experiments in cooperative human/robot force control for robot assisted microsurgical manipulation," in *Proc. IEEE Int. Conf. Robotics and Automation*, San Francisco, CA, Apr. 2000, pp. 610–617.

[14] P. J. Berkelman, L. L. Whitcomb, R. H. Taylor, and P. S. Jensen, "A miniature instrument tip force sensor for robot/human cooperative microsurgical manipulation with enhanced force feedback," in *Medical Image Computing and Computer-Assisted Interventions (MICCAI)*. Pittsburgh, PA: Springer, 2000, vol. 1935, Lecture Notes in Computer Science, pp. 897–906.

A New Robot Architecture for Tele-Echography

Adriana Vilchis, Jocelyne Troccaz, Philippe Cinquin, Kohji Masuda, and Franck Pellissier

***Abstract*—This paper presents a slave robot carrying an ultrasound probe for remote echographic examination. This robot is integrated in a master-slave system called robotic tele-echography (TER). The system allows an expert operator to perform a remote diagnosis from echographic data he acquires on a patient located in a distant place. The originality of this robot lies in its architecture: the cable-driven robot is lightweight and semirigid, and it is positioned on the patient body. In this paper, we describe the clinical application, the system architecture, the second implementation of the robot, and experiments performed with this prototype.**

***Index Terms*—Medical robotics, nonrigid robot, tele-echography.**

I. Introduction

Among many types of medical equipment, ultrasound (US) diagnostic systems are widely used because of their convenience and innocuity. Performing US examination involves good hand-eye coordination and the ability to integrate the acquired information over time and space; the physician has to be able to mentally build three-dimensional (3-D) information from both the two-dimensional (2-D) echographic images and the gesture information and to make a diagnosis from this information. Specialized physicians with these skills may be lacking in some healthcare centers or in emergency situations. Teleconsultation is, therefore, an interesting alternative to conventional care. Development of a high-performance remote diagnostic system, which enables an expert operator at the hospital to examine a patient at home, in an emergency vehicle, or in a remote clinic may have a very significant clinical added value.

In this domain, existing works can be structured in two subdomains: works exclusively related to the telemedicine aspect, mainly image transmission and manipulation (see, for instance, LOGINAT [1] and TeleinVivo [2]), and works integrating robotic assistance to the expert operator. A subclass of systems allows automating an echographic examination using a robot (see [3]–[5]). Finally, a second category of robot-based systems enables the remote examination of patients by a distant expert with [6], [7] or without [4], [8], [9] force feedback. Many of the robot-based systems integrate conventional robot architectures. However, medical robots belong to safety-critical systems. In such systems, the robot shares its working area with operators (medical staff) and has a close interaction with the patient. For echographic examinations, the robot is in contact with the body of the patient and imparts forces to it. Therefore, one major technical objective of this research was to propose a new architecture of low-weight, compliant, safe, and portable medical robots. The robotic tele-echography (TER)[1] system described in this paper belongs to the category of robotic-based systems with force feedback and includes a robot with an original kinematic architecture.

As can be seen, several systems are being developed worldwide to provide remote echographic examinations. None of them has yet been proven to answer this problem in a superior way to its competitors. [4] and [5] must be highlighted since they present a large range of control schemes enabling shared control, force control, visual servoing, and teleoperation. The main originality of TER lies in its robot architecture. As in [4], [5], [8], and [9], one objective was to design a light robot. The slave robot in Masuda's system is also lying on the patient's body and is the most similar to ours,[2] but differs in several ways: its user interface integrates two joysticks requiring teleoperating the robot in a decoupled way, it has no force feedback, and its robot is rigid. As compared with [7] which includes force feedback, one advantage of TER is that its slave robot architecture is more generic. For TER and Mitsuishi's systems, the haptic device is more sophisticated than strictly required by the application; this will be discussed later.

The main focus of this paper is the slave robot. Two prototypes were designed, realized, and experimented upon. The first prototype was based on pneumatic actuation with McKibben muscles and a slightly different kinematic architecture. Based on experimental work, we decided to modify the robot. The second prototype is described in this paper. We invite the interested reader to refer to cited papers for more details on the first prototype [10], force rendering [11], or telecommunication protocols [12]. The paper is organized as follows. Section II is devoted to the general presentation of the TER system, its general architecture, and operating mode. The clinical application constraints and the tele-echography protocol are described. Sections II–VI describe the slave robot. Section III focuses on the slave robot mechanical architec-

Manuscript received June 21, 2002; revised January 23, 2003 and June 18, 2003. This paper was recommended for publication by Editor R. Taylor upon evaluation of the reviewers' comments. This work was supported in part by the French Ministry of Research and Technology under RNRT project VTHD++, in part by France Telecom R&D, and in part by by UAEM-CONACYT Mexico. The work of K. Masuda was supported by the Toyobo Biotechnology Foundation.

A. Vilchis, J. Troccaz, P. Cinquin, and K. Masuda are with the IMAG-TIMC Laboratory, Computer-Aided Medical Interventions Team, 38706 La Tronche Cedex, France (e-mail: Jocelyne.Troccaz@imag.fr).

F. Pellissier is with France Telecom R&D, 38243 Meylan, France (e-mail: franck.pellissier@rd.francetelecom.com).

Digital Object Identifier 10.1109/TRA.2003.817509

[1]TER is a French acronym for robotic tele-echography.

[2]Those rather close robot mechanical designs were performed in parallel, each group independently of the other.